Self-assembly multifunctional DNA Tetrahedron for Efficient Elimination of Antibiotic-Resistant Bacteria

Yuhui Liao[1]

[1]Southern Medical University

June 1, 2023

Abstract

Antibiotic resistance is a major challenge in the clinical treatment of bacterial infectious diseases. Herein, we constructed a multifunctional DNA nanoplatform as a versatile carrier for bacteria-specific delivery of clinical antibiotic ciprofloxacin (CIP) and classic nanoantibiotic silver nanoparticles (AgNP). In our rational design, CIP was efficiently loaded in the self-assembly double-bundle DNA tetrahedron through intercalation with DNA duplex, and single-strand DNA-modified AgNP was embedded in the cavity of the DNA tetrahedron through hybridization. With the site-specific assembly of targeting aptamer in the well-defined DNA tetrahedron, the bacteria-specific dual-antibiotic delivery system exhibited excellent combined bactericidal properties. With enhanced antibiotic accumulation through breaking the out membrane of bacteria, the antibiotic delivery system effectively inhibited biofilm formation and promoted the healing of infected wounds in vivo. This DNA-based antibiotic delivery system provides a promising strategy for the treatment of antibiotic-resistant infections.

1

Aggregate

WILEY

Self-assembly multifunctional DNA Tetrahedron for Efficient Elimination of Antibiotic-Resistant Bacteria

Tiantian Wu[1, 2‡], Yu Fu[3‡], Shuang Guo[1‡], Yanqiang Shi[1], Yuxin Zhang[1], Zhijin Fan[1], Bin Yang[1]*, Baoquan Ding[2]* & Yuhui Liao[1]*

T. T. Wu, S. Guo, Y. Q. Shi, Y. X. Zhang, Z. J. Fan, B. Yang, Y. H. Liao
Molecular Diagnosis and Treatment Center for Infectious Diseases
Dermatology Hospital
Southern Medical University
Guangzhou 510091, China.
E-mail: yangbin1@smu.edu.cn; liaoyh8@mail.sysu.edu.cn.

T. T. Wu, Prof. B. Q. Ding
CAS Key Laboratory of Nanosystem and Hierarchical Fabrication
CAS Center for Excellence in Nanoscience
National Center for Nanoscience and Technology
11 BeiYiTiao, ZhongGuanCun, Beijing 100190, China
E-mail: dingbq@nanoctr.cn

Y. Fu
Longgang District Central Hospital of Shenzhen
Shenzhen, China.

Antibiotic resistance is a major challenge in the clinical treatment of bacterial infectious diseases. Herein, we constructed a multifunctional DNA nanoplatform as a versatile carrier for bacteria-specific delivery of clinical antibiotic ciprofloxacin (CIP) and classic nanoantibiotic silver nanoparticles (AgNP). In our rational design, CIP was efficiently loaded in the self-assembly double-bundle DNA tetrahedron through intercalation with DNA duplex, and single-strand DNA-modified AgNP was embedded in the cavity of the DNA tetrahedron through hybridization. With the site-specific assembly of targeting aptamer in the well-defined DNA tetrahedron, the bacteria-specific dual-antibiotic delivery system exhibited excellent combined bactericidal properties. With enhanced antibiotic accumulation through breaking the out membrane of bacteria, the antibiotic delivery system effectively inhibited biofilm formation and promoted the healing of infected wounds *in vivo*. This DNA-based antibiotic delivery system provides a promising strategy for the treatment of antibiotic-resistant infections.

1. Introduction

Bacterial infection has been considered to be the main cause of death and poses a tremendous threat to human health, which causes serious economic burdens worldwide.[1, 2] Although the fight against microorganism-caused infections has achieved considerable success since the discovery of antibiotics, the irrational use of antimicrobials which results in drug resistance has already caused serious medical problems and already attracted increasing concern.[3-5] Over the past few decades, significant progress has been achieved in the development of nanotechnology-based medicines for combating multidrug resistance in microorganisms.[6, 7] Nanoparticle-based antibiotic, such as silver nanoparticles (AgNP), with no cross-resistance to most of the chemically synthesized antibiotics, has attracted more attention in drug-resistant therapy.[8-10] Eventhough AgNP exhibits broad-spectrum and robust antimicrobial properties, it still holds the short back of instability in physiological environment and limited biosafety

caused by non-selectivity poisoning.[8, 10, 11] The hindrance in effective administration and target recognition restricts AgNPs from handling infectious problems physiologically.

DNA nanotechnology, which emerged at the beginning of the 1980s, generates new class of artificial medium to precisely control and organize functional ligands.[12-14] Precisely self-assembled DNA nanostructures, such as three-dimensional DNA tetrahedron, demonstrated excellent biocompatibility and high drug-loading capability and were used to efficiently enrich therapeutic drugs in the treatment of many kinds of diseases.[15-20] Due to excellent fabricability, the inner cavity of the DNA tetrahedron has been taken as a holder to deliver inorganic nanoparticles and protect them from inactivating by external biomolecules.[21, 22] Meanwhile, functional groups can be precisely organized on DNA tetrahedron to generate vital properties for specific recognition, such as antibody, peptide, and aptamer.[23-25] Through rational design, multifunctional DNA nanoplatforms could be integrated with multiple bioactive components to realize more excellent performance.[26, 27] Based on these tailored properties of DNA tetrahedron, we hypothesized that antibiotics-loaded multifunctional DNA nanoplatform could overcome dilemmas in antibiotic administration and realize effective antibiotic-resistant bacteria elimination.

Herein, we present a facile and universal strategy to deliver clinical antibiotic CIP and nanoantibiotic AgNP for targeted anti-infection therapy (Figure 1). An addressable double-bundle DNA tetrahedron (Th) is employed to load quinolone antimicrobial CIP[28-30] through noncovalent intercalation with DNA duplex. Meanwhile, AgNP modified with DNA was loaded in the Th with capture stretched from the inner cavity for the construction of the combined anti-bacterial therapy. For targeted delivery, the bacteria-specific aptamer was hybridized on the edge of the DNA tetrahedron (AT). The bacteria-specific dual antibiotics loaded DNA tetrahedron, namely AT-Ag@CIP, with the controlled size and high drug load efficacy, was successfully prepared and applied in infected wound therapy of resistant bacteria. The treatment of the AgNP-loaded DNA tetrahedron caused break in the integrity of the

bacterial membrane and synergistically enhanced the sterilization effect of the co-loaded drugs. The rationally designed DNA tetrahedron exhibits exceptional targetability and impressively bactericidal properties on antibiotic-resistant bacteria without observable toxicity. Consequently, our report demonstrated a combined anti-infection therapy agent that holds immense potential as treatment strategy for systematic infection.

2. Results and Discussion

2.1 Characterization of the antibiotic-loaded DNA tetrahedron

We constructed an addressable double-bundle DNA tetrahedron based on our previous studies as the drug carrier for antibiotic delivery (Figure S1). There are 6 capture strands stretched from 3 arms of the DNA tetrahedron for AgNP binding and the bacteria-specific aptamer was loaded through hybridization on the opposite side (Figure S2-S5, detailed DNA sequences are shown in Table S1). We employed AgNP with a 5 nm diameter as nanoantibiotic for ^{A}T-Ag@CIP preparation (Figure S6). The DNA-modified AgNP (Ag-DNA) was loaded, meanwhile, the clinical antibiotic CIP was loaded through intercalation with DNA duplex of the double-bundle DNA tetrahedron (Figure S7). HPLC analysis showed that there are about 457.5 ± 17.5 CIP molecules loaded in each DNA tetrahedron. The noncovalent drug loading strategy of intercalation had a relatively high drug loading efficiency through single coculture as reported.[31, 32] After two steps of ^{A}Th fabrication and one step of drug loading, the morphology and size distribution were obtained by atomic force microscopy (AFM) and dynamic light scattering (DLS) (Figure 2A). A monodisperse antibiotic-loaded DNA tetrahedron was successfully synthesized. There is no aggregation or disassembly was observed during the CIP and AgNP loading (Figure S8). The diameter of the antibiotic-loaded ^{A}Th-Ag@CIP (15.9 ± 5.3 nm) is slightly larger than that of ^{A}Th (13.3 ± 2.7 nm) due to the successful antibiotic loading.

Then, the drug release efficacy and physiological stability were subsequently investigated. We found that the drug release behavior of ^{A}T-Ag@CIP was in a time-dependent manner in all tested pH conditions. The CIP and antibacterial Ag^+ were sustained-released into the external environment over 48 h (Figure 2B-C). The addition of rhDNase caused a suddenly released of CIP, indicating the interaction with DNA carrier maintained the sustained release of CIP (Figure S9). Next, the tolerance of AgNPs was applied to test the stability of ^{A}T-Ag@CIP in PBS. The 5 nm AgNP has a larger surface area for efficient Ag^+ hydrolysis so that achieves a better antibacterial effect.[6, 33] However, the shortage of limited stability in physiological conditions extremely limited its application. As shown in Figure S10, the naked AgNP aggregated in PBS after 12 h of culture, while the ^{A}Th-Ag@CIP had negligible morphological change according to AFM images. The strategy of taking DNA tetrahedron as drug carrier apparently improved the applied performance of the antibiotics.

2.2 *In vitro* drug delivery performance of the dual-antibiotic delivery system

To investigate the cellular uptake efficiency of antibiotics delivered by DNA tetrahedron, we employed Cy5-labeled DNA strands (red) for confocal imaging analysis. Escherichia coli (*E. coil*) as one of the most prevalent pathogens in infectious diseases is increasingly involved in clinical infection.[34, 35] We first chose anti-*E. coil* aptamer to equip the DNA tetrahedron (^{A}Th) and the *in vitro* binding and antibiotic delivery performance was explored. As shown in Figure 3A, ^{A}Th showed the greatest affinity to bacteria, whereas a slightly detectable fluorescence signal was observed in ssDNA and Th treatment. Then, we analyzed the incell accumulation of the antibiotics. The HPLC analysis (experimental condition is shown in Table S2) showed that compared to free CIP and nontargeted delivery of CIP, the ^{A}T@CIP treatment significantly enhanced the accumulation of CIP in *E. coil* (Figure 3B). Consistent results were obtained in the cell Ag (including AgNP, Ag^+, and biomolecular adducts containing Ag) quantification test by ICP-MS. The highest Ag accumulation by ^{A}T-Ag treatment reached up to 4.6 times higher

than AgNP treatment (Figure 3C). After testing the performance of the targeted delivery system on antibiotics delivery, we investigated the effect of free antibiotics and delivery system on the cellviability of different cell lines (HaCat, L929, HUVEC, RSC 96, and Raw). As shown in Figure 3D and Figure S11, the DNA tetrahedron reduced the killing effects of CIP and AgNP on mammalian cells, indicating excellent biocompatibility of the DNA tetrahedron-based antibiotic carrier.

2.3 Anti-bacterial effect of the dual-antibiotic delivery system

We then tested the anti-bacterial effect of the dual-antibiotic delivery system. As presented in Figure 4A, the Live/Dead staining and related quantification revealed that Th-Ag@CIP and [A]T-Ag@CIP significantly induced bacteria death. More than 50.2% of bacteria were killed after the treatment of [A]T-Ag@CIP. Furthermore, the growth curve of *E. coil* treated with the antibiotic mixture or dual-antibiotic delivery system furtherly revealed that the strategy of co-delivery of CIP and AgNP could apparently improve the therapeutic effect of the antibiotics (Figure 4B). The addition of two antibiotics simultaneously inhibited the proliferation of the bacteria, impressively, the [A]T-Ag@CIP thoroughly cleared the bacteria in the test (Figure S12). To expand the application of the targeted antibiotic delivery system, we changed the sequence of the bacteria-specific aptamer to explore the bactericidal effect on variety of species of bacteria. Instead of the *E. coil*-specific aptamer A, the *S. aureus*-specific aptamer A' was modified to prepare [A']T-Ag@CIP for Gram+ *S. aureus* caused infection, and the *P aeruginosa*-specific aptamer A'' was modified to prepare [A'']T-Ag@CIP for another Gram- *P. aeruginosa* caused infection (Figure 4C). CIP is broadly applied in various infectious diseases through taking A subunit of the essential enzyme DNA gyrase as the target, while the CIP resistance that occurred in first-line treatment is now rising among systemic infectious diseases.[36, 37] The excellent bactericidal activity of the [A]T-Ag@CIP inspired us to apply these bacteria-specific dual-antibiotic delivery systems for resistant bacteria killing. The induction and culture of CIP-

resistant bacteria were conducted through adding increased concentration of CIP into the culture medium as shown in Figure S13A. The minimum inhibitory concentration (MIC) of the bacteria on CIP increased from 0.5 μM (*E. coli*), 1.0 μM (*S. aureus*), and 2.0 μM (*P. aeruginosa*) to 4.0 μM (CIP resistant *E. coli*: CREC), 8.0 μM (CIP resistant *S. aureus:* CRSA), and 8.0 μM (CIP resistant *P. aeruginosa:* CRPA) (Figure S13B). After the induction, the tolerance of 3 kinds of bacteria to CIP significantly increased.

Then we applied DNA tetrahedron, CIP+AgNP, Th-Ag@CIP, and aptamer-modified antibiotic delivery system on bactericidal test. According to Figure 4C, the aptamer-modified DNA tetrahedron had no effect on bacterial growth. The drug mixture CIP+AgNP depressed the proliferation of all of the bacteria strains, however, a reduced inhibition effect was observed when the mixture was applied to CIP-resistant strains. Apparently, the strategy of the antibiotic co-delivery significantly enhanced the bacterial elimination effect, especially when the antibiotic carrier was modified with bacteria-specific aptamer. On bacterial elimination effect, the ^{A}T-Ag@CIP, $^{A'}$T-Ag@CIP, and $^{A''}$T-Ag@CIP achieved 6.1, 6.0, and 4.2 times higher than antibiotic mixture on CIP-sensitive bacteria and 5.5, 3.8, and 3.2 times higher than antibiotic mixture on CIP-resistant bacteria separately. In nanoantibiotic treatments, AgNP without modification showed a slight inhibition effect on all of the bacteria strains (Figure S14). The defect of poor stability in physiological environment restricts the application of the AgNP in sterilization.[38-40] With protection and guidance from DNA tetrahedron, the ^{A}T-Ag, $^{A'}$T-Ag, and $^{A''}$T-Ag showed a notably increased antibacterial effect on all bacteria strains. Furthermore, free CIP had barely no inhibition effect on resistant bacteria, while the ^{A}T@CIP, $^{A'}$T@CIP, and $^{A''}$T@CIP effectively restrained the growth of CREC, CRSA, and CRPA. Agar plate diffusion assay was also rendered for testing the sterilization effect. Different drugs were added in the hole punched in the agar plate containing bacteria and the inhibition zone was measured after incubation (Figure 5). The largest inhibition zone caused by ^{A}T-Ag@CIP, $^{A'}$T-Ag@CIP, and $^{A''}$T-Ag@CIP indicates the powerful antibacterial of the targeted dual-antibiotic delivery system.

In summary, the bacteria-specific dual-antibiotic delivery system enhanced the antibacterial effect of the loaded antibiotics, especially in antibiotic-resistant bacteria treatment.

2.4 Antibacterial mechanism of ^AT-Ag@CIP

Following the assessment of the bactericidal effect, we analyzed the antibacterial mechanism of ^AT-Ag@CIP on CIP-resistant strain CREC. Since the resistance of synthetic antibiotics mostly relates to the decrease in the accumulation of drugs in bacteria, the permeation barriers are critical for the effect of antibiotics.[4, 41, 42] The Ag$^+$ hydrolyzed from nanoantibiotic AgNP has multiple mechanisms in antibacterial application, including disrupting membrane and leakage of intracellular content, affecting permeation, and damaging bacterial DNA.[38, 43] Therefore, the combination of destroying the membrane of bacteria and increasing the transmembrane of antibiotics may overcome antimicrobial resistance. As illustrated in Figure 6A, the targeted dual-antibiotic delivery system exerts bacteriostatic effect through synergistic killing followed specific recognition. To observe the detailed action of ^AT-Ag@CIP in the membrane of the antibiotic-resistant bacteria, we utilized scanning electron microscopy (SEM) for the investigation of the disruption of the membrane. A clear rod shape with an integrated surface was observed for CREC treated with PBS and ^ATh (Figure 6B). In contrast, significant morphology changes were observed in ^AT-Ag@CIP treated CREC, barely no contact structure can be observed in the field of the SEM image. The antibiotics mixture only caused a slight collapse in the cell structure as the red arrows indicated, which was mainly realized by the disruption effect of Ag$^+$ on bacterial out structure (Figure S15). To confirm the mechanism of membrane disruption, the ONPG assay was utilized for membrane permeability analysis. β-galactosidase leaked from bacteria cytoplasm can turn ONPG into yellow product for the quantification of bacterial content leakage (Figure S16). As shown in Figure 6C, remarkably increased leakage was measured in the ^AT-Ag@CIP treated group. The leaked K$^+$ and alkaline phosphatase (AKP) were also measured to further quantitatively assess the leakage and evaluate

permeability (Figure 6D-E). Consistent with the results of ONPG test, the [A]T-Ag@CIP treatment led to the highest leakage of K^+ and AKP from CREC cells. Compared with the antibiotic mixture group, the significantly increased leakage demonstrated that the targeted co-delivery of the antibiotics can more effectively destroy the bacterial structure.

2.5 Anti-biofilm effect of the dual-antibiotic delivery system

Biofilm as dominant form of bacterial growth is aggregates of bacteria and extracellular matrices of macromolecules that provides protection for the resident microorganisms in infections.[44, 45] Unlike the planktonic state, bacteria in biofilms are wrapped up with self-produced matrix, rendering them resilient to antibiotics through reducing the penetration of antibiotics.[46, 47] Various materials have been developed and applied for biofilm clearance, eventhough, biofilm-associated infections still hold particularly challenging problems, especially in antibiotic resistance. In order to evaluate the anti-biofilm formation effects of the bacteria-specific dual-antibiotic delivery system, we conducted biofilm imaging by staining the samples with a bacterial Live/Dead staining kit. As shown in Figure 7A, CREC treated with PBS, AgNP, CIP ointment, AgNP+CIP mixture, Th-Ag@CIP, and [A]T-Ag@CIP were cultured for biofilm formation. Intensive green fluorescence represented successful formation of biofilm in PBS control. The [A]T-Ag@CIP treatment caused largely death (red signal) of bacteria and showed the strongest inhibition effect in restraining biofilm formation. Then, we applied different drugs in the biofilm inhibition test to furtherly evaluate the anti-biofilm efficacy. The degradation of the biofilm was visualized by crystal violet staining and then optical density measurements were used for quantitative analysis (Figure 7B). It is worth mentioning that the antibiotic mixture showed slight disruption in biofilms, especially in the antibiotic-resistant strain. However, when CIP and AgNP were delivered simultaneously, the residual biofilms decreased gradually on both CIP-sensitive *E. coil* and CIP-resistant CREC. The modification of bacteria-specific aptamer especially enhanced the inhibition effect with a decrease in the

formation rate to 12.3% for CIP-sensitive *E. coli* and 15.8% formation for CIP-resistant CREC. Next, we test biofilm formation-related self-aggregation on both two kinds of bacteria (Figure 7C). Significant inhibition effect was found on both two strains after being treated with [A]T-Ag@CIP (average inhibition rate: 66.7% in *E. coil* and 68.7% in CREC). As an important indicator in biofilm formation, the break of aggregation of bacteria is of great significance in biofilm inhibition.[48, 49] The bacteria-specific dual-antibiotic delivery system with powerful antibacterial efficacy holds great potential in the application of biofilm clearance.

2.6 *In vivo* anti-infection effect of the dual-antibiotic delivery system

The excellent antibacterial activity of the dual-antibiotic delivery system *in vitro* encouraged us to study the anti-infection therapy effect *in vivo*. The antibiotic-resistant *E. coil K12 J53* (BNCC361521) was used to establish infected wound models in BALB/c mice. The infected wounds were administered with PBS, [A]Th, Ag+CIP, Th-Ag@CIP, and [A]T-Ag@CIP by directly dripping on wounds at 6 h after infection. The wound healing was monitored photographically as shown in Figure 8A. The wound size gradually reduced on day 8 after the treatment of dual-antibiotic delivery system (Figure 8B). On day 12, the administration of [A]T-Ag@CIP elicited the highest wound closure. Only 5.4% wound area was measured after the treatment of [A]T-Ag@CIP, which is remarkably lower than Th-Ag@CIP treatment. In contrast, the wound treated with PBS and [A]Th remained 40.1% and 42.0% wound area, separately (Figure S17). These results demonstrated that the modification of targeted aptamer is crucial for [A]T-Ag@CIP in efficiently kill pathogens and accelerate the process of wound healing.

After different treatments, bacteria at wound were detected by the agar plate to evaluate the bactericidal effect of the dual-antibiotic delivery system. As shown in Figure 8C, a large number of bacteria on the agar plates of the PBS group were observed. As expected, the number of bacteria decreased through the treatment of the delivery system. The [A]T-Ag@CIP group displayed almost no bacteria on the agar plate, which demonstrate an obvious antimicrobial

capacity *in vivo*. In infected wounds, the reactive oxygen species (ROS) is consistent with inflammation caused by bacterial infection.[50, 51] In the ROS quantitative imaging test, As expected, a dramatically diminished red fluorescence was observed in ^{A}T-Ag@CIP group. In summary, the bacteria-specific dual-antibiotic delivery system ^{A}T-Ag@CIP holds powerful antibacterial efficacy in infected wound healing.

3. Conclusion

In this study, we successfully constructed a bacteria-specific dual-antibiotic delivery nanoplatform to transport clinical antibiotic CIP and classic nanoantibiotic AgNP for antibiotic-resistant infection therapy *in vivo*. This structurally well-defined DNA nanocarrier demonstrated several unique advantages for targeted antibiotics delivery. Firstly, the addressable double-bundle DNA tetrahedron is suitable to arrange bacteria-specific aptamer to binding with specific pathogenic bacteria. Secondly, the multifunctional DNA nanocarrier is tailored for loading CIP through intercalation with DNA duplex and holding DNA-modified AgNP into the cavity through DNA hybridization. Finally, dual-antibiotic loaded DNA nonoplatform can realize combined antibacterial therapy with bacteria-specific recognition. After the treatment of ^{A}T-Ag@CIP on antibiotic-resistant infection, we observed powerful antibacterial effect with deformed and broken bacterial structure, noticeable clearance of the resistant biofilm, and rapid healing of infected wounds. This dual-antibiotic delivery system can be developed into a versatile platform to transport other functional components such as therapeutic genes and protein drugs for antibacterial treatment. We believe this multifunctional DNA nanoplatform will open a new avenue for targeted anti-infection therapy.

4. Experimental Section

4.1 Assembly of DNA Tetrahedron

Nucleic acid sequences for the assembling of the ^{A}Th in this work were shown in Table S1. The purchased DNA strands were dissolved in ddH$_2$O. The denatured PAGE was employed for

further purification of DNA strands. The final concentration was measured by Nanodrop. Firstly, the purified DNA strands (100 nM) of each Y-shape motif (V1, V2, V3, and V4) were equally mixed in a 1×TAE/Mg^{2+} buffer (pH = 8.3), respectively. The aforementioned assembly samples were kept at 95 °C (5 min) and then cooled down to 37 °C for 1 h. Then four Y-shape motifs and aptamer DNA hybrids were assembled with a molecular ratio of 1:1:1:1:3. Then the mixture was cooled down from 37 to 25 °C in 12 h and stored at 4 °C.

4.2 Construction of the ^{A}Th-Ag@CIP

The synthesis of AgNP followed the procedure reported by S. Agnihotri and coworkers[6, 52] with some changes, and the modification of AgNP with DNA strand was according to the original procedure presented by *S. Pai*.[53] Briefly, the AgNP colloid synthesized by NaBH4 and TSC reduction was concentrated by centrifugation (8,000 rpm, 40 min) and re-dispersed in 1 x TBE buffer in the dark. Cap-Ag (8 μM) with 9 ps backbone modified base was added to the AgNP solution and cultured overnight. Then 4 M NaCl was added to raise the final NaCl concentration to 350 mM and the solution was kept shaking at room temperature for 12 h. Then the excess of Cap-Ag was removed by centrifugation.

The pre-assembled DNA tetrahedron (100 nM) was mixed with Ag-DNA at a molecular of 1:1. Then the mixture was added with CIP and furtherly cultured at room temperature for 9 h in the dark. After the loading process, the residual drug was removed using Amicon stirred cell (UFSC05001) equipped with 3 kDa filter (PLHK04310). The ^{A}Th and ^{A}Th-Ag@CIP were imaged with a MultiMode 8 atomic force microscopy (Bruker) under ScanAsyst-Fluid mode on mica. Dynamic light scattering (DLS) of DNA tetrahedron (20 nM) was measured by the Malvern Zetasizer Nano-ZS (U.K.).

4.3 Cellular internalization analysis

For bacterial binding test, 100 μL of *E. coli* solution (10^9 CFU/mL) was added into 900 μL of PBS solution with Cy5 modified ssDNA (ssDNA^{Cy5}) or Cy5 labeled DNA tetrahedron (Th^{Cy5}

or ^{A}Th^{Cy5}) to get the final concentration of 100 nM DNA tetrahedron. Then the mixture was incubated at 37 °C for 15 min in the dark and collected by centrifugation (5000 rpm, 1 min). The bacteria were added to a clean glass slide and immobilized with a glass coverslip for CLSM (Carl Zeiss, Jena, Germany) observation.

For the measurement of CIP in bacteria, activated *E. coli* solution (10^9 CFU/mL) was transferred to 6-well plates and incubated with CIP, Th@CIP, and ^{A}Th@CIP 37 °C for 0.5 h. Then, the suspension was centrifuged and washed with PBS for 3 times. The concentration of the antibiotic was determined by HPLC analysis. For the measurement of Ag in bacteria, activated *E. coli* solutions were incubated with AgNP, Th-Ag, and ^{A}Th-Ag at the final concentration of 50 nM AgNP at 37 °C for 2 h. After cell counting, the harvested bacteria were digested with nitric acid/aqua regia for ICP-MS measurement.

4.4 Bacterial Apoptosis Assay

The drugs and drug mixture were incubated with *E. coli* (10^5 CFU/mL) at 37 °C for 2 h. Then the samples were collected (5000 rpm, 1 min) and resuspended with PBS. After that, the treated *E. coli* were stained with DMAO (Ex/Em=503/530 nm) and EthD-III (Ex/Em=530/620 nm) of the Live & Dead Bacterial Staining Kit (Yeasen Biotech Co., Ltd.). Then 5 μL of each sample was used for CLSM observation.

4.5 Induction of the CIP-resistant bacteria

The monoclonal of the bacteria was transferred into 3 mL Mueller-Hinton (MH) broth. The culture was incubated at 37 °C at 220 rpm until OD$_{600}$ reached 0.4~0.6. Then spread the bacterial culture out on MH-agar plate containing CIP. The initial concentration of CIP is half of the MIC of the bacterial strains. Subsequently, the concentration of CIP was doubled in each induction cycle. After 5 rounds of induction, the CIP-resistant bacteria were consecutively cultured for 5 times to ensure stable inheritance of drug resistance. Then the MIC was measured to verify the drug resistance.

4.6 Antimicrobial activity tests

The drug-treated bacteria were resuspended to reach a final cell density of 10^6 CFU/mL using LB broth. Subsequently, the drugs were added, and the mixture was transferred into a 24-well plate. After 12 h incubation, 10 μL bacterial suspensions were obtained and evenly dispersed on LB-agar plate.

In the agar diffusion test, 200 μL of the bacterial suspension (10^5 CFU/mL) was added into and spread out on LB-agar plate surface. Then, a hole about 1 mm in diameter was punched and fulfill with 5 μL test compounds. The dishes were incubated overnight at 37 °C. The zone of inhibition was evaluated by measuring the diameter of the bacterial growth inhibition zone around the membrane in millimeters.

4.7 Morphological observation of bacterial structure

The CIP-resistant CREC treated with different drugs were collected and washed with PBS for 3 times. Then, the bacteria were fixed overnight in 4% paraformaldehyde at 4 °C, dehydrated with anhydrous ethanol concentration gradient, and then dried in vacuum. Then the samples were coated with gilded film before imaging by electron microscope (Hitachi S4800+EDS).

4.8 Membrane permeability assay

To investigate inner membrane permeability, the activity of cytoplasmic β-galactosidase from *E. coli* was measured using ONPG.[20, 54] Briefly, the activated *E. coli* (10^6 CFU/mL) were treated with different drugs and incubated with ONPG (300 μg/ml) for 0.5 h at 37 °C in a 96-well plate. Subsequently, the indicator product ONP was determined by measuring the absorbance at 420 nm (Varioskan®LUX, Thermo Scientific, USA). To investigate the leakage of cell content of the bacteria, *E. coli* (10^6 CFU/mL) treated with drugs were centrifuged and filtrated to obtain the supernatants. Subsequently, the obtained supernatants were analyzed through colorimetric detection kit to quantify the content of K^+ and alkaline phosphatase (GENMED).

4.9 Biofilm formation test

Bacteria were cultured in agar plate containing 1 ml of broth supplemented with drugs. After 12 h of growth, the broth was carefully removed, and 0.5 mL of PBS was added into the dish. The bacteria were scraped from the surface using a cell scraper and transferred to a 1.5 mL tube. Then the samples were resuspended by gentle pipetting and the tubes were then incubated statically for 10 min. The OD_{600} of the supernatant was measured for auto-aggregation analysis.

E. coli and CREC (10^6 CFU/mL) were pipetted into 48-well plates and incubated at 37 °C for 12 h. LB broth supplemented with drugs was added to the wells and incubated for another 24 h in static conditions. For fluorescence imaging, Live/Dead staining kit was added, and the mixture was cultured for 15 min in the dark for fluorescence microscope observation. For crystal violet stain, the plates were then washed vigorously by submersion in ddH_2O and left to dry for 15 min at room temperature. Crystal violet solution (1 mL of 0.1 wt %) was added and incubated for 15 min. After washed thoroughly with ddH_2O, the plate was left to dry for 2 h. Acetic acid (1 mL, 30 wt %) was added to each well to solubilize the crystal violet. This solution was measured at 570 nm with 30 wt % acetic acid used as blank.

4.10 *In Vivo* Antibacterial Study

All animals received care in compliance with the guidelines outlined in the Guide for the Care and Use of Laboratory Animals. The procedures were approved by the Institutional Animal Care and Use Committee of the Institute of Zoology, Chinese Academy of Sciences. The Balb/c mice (6 weeks old) mice (20-25 g) were anesthetized and full-thickness cutaneous wound (6 mm×6 mm) area was created on the back. Then, 10 μL of bacterial solution (1×10^7 CFU/mL) was introduced onto the wound. Then, the mice were randomly divided into 5 groups (n=5) and treated with different drugs at 6 h after the infection. To observe the wound healing process, wounds were photographed at Day 0, 4, 8, and 12. Wound healing rates were calculated according to the equation:

$$\text{Relative wound area} = \frac{\text{Wound area at certain day}}{\text{Wound area at day 0}} \times 100\%$$

(1)

To measure the amount of bacteria in the infected tissues, the tissues were homogenized, diluted with PBS, and then plated on LB-agar plate for 16 h. The viable bacteria were observed and photographed.

4.11 Statistical Analysis

The data from one representative experiment among at least three independent experiments are expressed as the mean ± SEM. One-way ANOVA followed by Tukey multiple comparisons was used to determine the statistical differences between the groups. Quantitative data are presented as mean S.D. $*P < 0.05$, $**P < 0.01$, $***P < 0.001$, and $****P < 0.0001$ were considered statistically significant. Statistical analysis was conducted using GraphPad Prism software (version 8.02).

Author Contributions

Tiantian Wu: Conceptualization, Methodology, Software, Data curation, Writing-original draft. **Yu Fu**: Visualization, Methodology, Data curation, Writing-original draft preparation. **Shuang Guo**: Resources, Supervision. **Yanqiang Shi**: Methodology, Software, Data curation. **Yuxin Zhang**: Visualization. **Zhijin Fan**: Software, Methodology. **Jianbing Liu**: Methodology, Writing Reviewing and Editing. **Bin Yang**: Funding acquisition, Writing-reviewing, and editing. **Baoquan Ding**: Funding acquisition, Writing-reviewing & editing. **Yuhui Liao**: Writing-reviewing & editing, Supervision, Funding acquisition, Project administration.

Tiantian Wu, Yu Fu, and **Shuang Guo** contributed equally to this work. All authors have given approval to the final version of the manuscript.

Conflict of Interests

The authors declare no conflict of interests.

Data Availability Statement

The data that support the findings of this study are available from the corresponding author upon reasonable request.

Supporting Information

Supporting Information is available from the Wiley Online Library or from the author.

<div align="right">

Received: ((will be filled in by the editorial staff))
Revised: ((will be filled in by the editorial staff))
Published online: ((will be filled in by the editorial staff))

</div>

References

1. R. E. Baker, A. S. Mahmud, I. F. Miller, M. Rajeev, F. Rasambainarivo, B. L. Rice, S. Takahashi, A. J. Tatem, C. E. Wagner, L.-F. Wang, A. Wesolowski, C. J. E. Metcalf, *Nat. Rev. Microbiol.* **2022**, *20*, 193.

2. A. R. Kirtane, M. Verma, P. Karandikar, J. Furin, R. Langer, G. Traverso, *Nat. Nanotechnol.* **2021**, *16*, 369.

3. E. K. Perry, L. A. Meirelles, D. K. Newman, *Nat. Rev. Microbiol*. **2022**, *20*, 129.

4. J. M. V. Makabenta, A. Nabawy, C.-H. Li, S. Schmidt-Malan, R. Patel, V. M. Rotello, *Nat. Rev. Microbiol.* **2021**, *19*, 23.

5. W. Gao, L. Zhang, *Nat. Rev. Microbiol.* **2021**, *19*, 5.

6. S. Tang, J. Zheng, *Adv. Healthc. Mater*. **2018**, 7, 1701503.

7. S. E. Birk, A. Boisen, L. H. Nielsen, *Adv. Drug Delivery Rev.* **2021**, *174*, 30.

8. L. M. Stabryla, K. A. Johnston, N. A. Diemler, V. S. Cooper, J. E. Millstone, S.-J. Haig, L. M. Gilbertson, *Nat. Nanotechnol.* **2021**, *16*, 996.

9. S. Kumar, R.K. Majhi, A. Singh, M. Mishra, A. Tiwari, S. Chawla, P. Guha, B. Satpati, H. Mohapatra, L. Goswami, C. Goswami, *ACS Appl. Mater. Inter.* **2019**, *11*, 42998.

10. H. Zhao, M. Wang, Y. Cui, C. Zhang, *Environ. Sci. Technol.* **2022**, *56,* 5090.

11. A. Panáček, L. Kvítek, M. Smékalová, R. Večeřová, M. Kolář, M. Röderová, F. Dyčka, M. Šebela, R. Prucek, O. Tomanec, R. Zbořil, *Nat Nanotechnol*. **2018**, *13*, 65.

12. N.R. Kallenbach, R.-I. Ma, N.C. Seeman, *Nature* **1983**, *305*, 829.

13. R.P. Goodman, I.A.T. Schaap, C.F. Tardin, C.M. Erben, R.M. Berry, C.F. Schmidt, A.J. Turberfield, *Science* **2005**, *310*, 1661.

14. A.V. Pinheiro, D. Han, W.M. Shih, H. Yan, *Nat. Nanotechnol.* **2011**, *6*, 763.

15. N.C. Seeman, H.F. Sleiman, *Nat. Rev. Mater.* **2017**, *3*, 17068.

16. Y. He, T. Ye, M. Su, C. Zhang, A.E. Ribbe, W. Jiang, C. Mao, *Nature* **2008**, *452*, 198.

17. Q. Hu, H. Li, L. Wang, H. Gu, C. Fan, *Chem. Rev.* **2019**, *119,* 6459.

18. S. Dey, C. Fan, K.V. Gothelf, J. Li, C. Lin, L. Liu, N. Liu, M.A.D. Nijenhuis, B. Saccà, F.C. Simmel, H. Yan, P. Zhan, *Nat. Rev. Methods Primers* **2021**, *1*, 13.

19. H. Liang, X.-B. Zhang, Y. Lv, L. Gong, R. Wang, X. Zhu, R. Yang, W. Tan, *Acc. Chem. Res*. **2014**, *47*, 1891.

20. Y. Sun, Y. Liu, B. Zhang, S. Shi, T. Zhang, D. Zhao, T. Tian, Q. Li, Y. Lin, *Bioact. Mater.* **2021**, *6*, 2281.

21. A. Qu, X. Wu, S. Li, M. Sun, L. Xu, H. Kuang, C. Xu, *Adv. Mater.* **2020**, *32*, 2000184.

22. T. Wu, Q. Liu, Y. Cao, R. Tian, J. Liu, B. Ding, *ACS Appl. Mater. Inter.* **2020**, *12*, 32461.

23. S. Liu, Q. Jiang, X. Zhao, R. Zhao, Y. Wang, Y. Wang, J. Liu, Y. Shang, S. Zhao, T. Wu, Y. Zhang, G. Nie, B. Ding, *Nat. Mater.* **2021**, *20*, 421.

24. J. Liu, L. Song, S. Liu, S. Zhao, Q. Jiang, B. Ding, *Angew. Chem. Int. Ed.* **2018**, *57*, 15486.

25. Y. Xu, S. Jiang, C.R. Simmons, R.P. Narayanan, F. Zhang, A.-M. Aziz, H. Yan, N. Stephanopoulos, *ACS Nano*, **2019**, *13*, 3545.

26. H. Lee, A.K. Lytton-Jean, Y. Chen, K.T. Love, A.I. Park, E.D. Karagiannis, A. Sehgal, W. Querbes, C.S. Zurenko, M. Jayaraman, C.G. Peng, K. Charisse, A. Borodovsky, M. Manoharan, J.S. Donahoe, J. Truelove, M. Nahrendorf, R. Langer, D.G. Anderson, *Nat. Nanotechnol.* **2012**, *7*, 389.

27. S. Zhao, R. Tian, J. Wu, S. Liu, Y. Wang, M. Wen, Y. Shang, Q. Liu, Y. Li, Y. Guo, Z. Wang, T. Wang, Y. Zhao, H. Zhao, H. Cao, Y. Su, J. Sun, Q. Jiang, B. Ding, *Nat. Commun.* **2021**, *12*, 358.

28. J.S. Wolfson, D.C. Hooper, *Clin. Microbiol. Rev.* **1989**, *2*, 378.

29. R. Davis, A. Markham, J. A. Balfour, *Drugs* **1996**, *51*, 1019.

30. S. Hernando-Amado, P. Laborda, J. R. Valverde, J. L. Martínez, *Proc. Natl. Acad. Sci. USA* **2022**, *119*, 2109370119.

31. T. Wu, J. Liu, M. Liu, S. Liu, S. Zhao, R. Tian, D. Wei, Y. Liu, Y. Zhao, H. Xiao, B. Ding, *Angew. Chem. Int. Ed.* **2019**, *58*, 14224.

32. J. Liu, L. Song, S. Liu, Q. Jiang, Q. Liu, N. Li, Z.-G. Wang, B. Ding, *Nano Lett*. **2018**, *18*, 3328.

33. Z.M. Xiu, Q.B. Zhang, H.L. Puppala, V.L. Colvin, P.J. Alvarez, *Nano Lett*. **2012**, *12*, 4271.

34. E. Denamur, O. Clermont, S. Bonacorsi, D. Gordon, *Nat. Rev. Microbiol.* **2021**, *19*, 37

35. L. H. Caitlyn, T. A. Mark, L. T. M. Harry, A. B. Michael, *Clin. Microbiol. Rev.* **2021**, *34*, 00234-20.

36. A.H. Holmes, L.S.P. Moore, A. Sundsfjord, M. Steinbakk, S. Regmi, A. Karkey, P.J. Guerin, L.J.V. Piddock, *The Lancet* **2016**, *387*, 176.

37. J.C. Nwabuife, C.A. Omolo, T. Govender, *J. Control. Release* **2022**, *349*, 338.

38. B. Le Ouay, F. Stellacci, *Nano Today* **2015**, *10*, 339.

39. L. Liu, W. Li, X. He, J. Yang, N. Liu, *Small* **2022**, *18*, 2104205.

40. D. Panacek, L. Hochvaldova, A. Bakandritsos, T. Malina, M. Langer, J. Belza, J. Martincova, R. Vecerova, P. Lazar, K. Polakova, J. Kolarik, L. Valkova, M. Kolar, M. Otyepka, A. Panacek, R. Zboril, *Adv. Sci.* **2021**, *8*, 2003090.

41. H.S. Gold, R.C. Moellering, *New Engl. J. Med.* **1996**, *335*, 1445.

42. D.G.J. Larsson, C.-F. Flach, *Nat. Rev. Microbiol.* **2022**, *20*, 257.

43. A. Gupta, S. Mumtaz, C.-H. Li, I. Hussain, V.M. Rotello, *Chem. Soc. Rev.* **2019**, *48*, 415.

44. H.C. Flemming, J. Wingender, U. Szewzyk, P. Steinberg, S.A. Rice, S. Kjelleberg, *Nat. Rev. Microbiol.* **2016**, *14*, 563.

45. K. Sauer, P. Stoodley, D.M. Goeres, L. Hall-Stoodley, M. Burmølle, P.S. Stewart, T. Bjarnsholt, *Nat. Rev. Microbiol.* **2022**, *20*, 608.

46. Y. Liu, L. Shi, L. Su, H.C. van der Mei, P.C. Jutte, Y. Ren, H.J. Busscher, *Chem. Soc. Rev.* **2019**, *48*, 428.

47. S. Darvishi, S. Tavakoli, M. Kharaziha, H.H. Girault, C.F. Kaminski, I. Mela, *Angew. Chem. Int. Ed.* **2021**, *61*, 202112218.

48. J. Li, H. Shen, H. Zhou, R. Shi, C. Wu, P.K. Chu, *Mat. Sci. Eng. R.* **2023**, *152*, 100712.

49. Z.-R. Li, J. Sun, Y. Du, A. Pan, L. Zeng, R. Maboudian, R.A. Burne, P.-Y. Qian, W. Zhang, *Nat. Chem. Biol.* **2021**, *17*, 576.

50. C. Tu, H. Lu, T. Zhou, W. Zhang, L. Deng, W. Cao, Z. Yang, Z. Wang, X. Wu, J. Ding, F. Xu, C. Gao, *Biomaterials* **2022**, *286,* 121597.

51. H. Zhao, J. Huang, Y. Li, X. Lv, H. Zhou, H. Wang, Y. Xu, C. Wang, J. Wang, Z. Liu, *Biomaterials* **2020**, *258,* 120286.

52. S. Agnihotri, S. Mukherji, S. Mukherji, *RSC Advances*, **2014**, *4*, 3974.

53. S. Pal, Z. Deng, B. Ding, H. Yan, Y. Liu, *Angew Chem. Int. Ed.* **2010**, *49*, 2700.

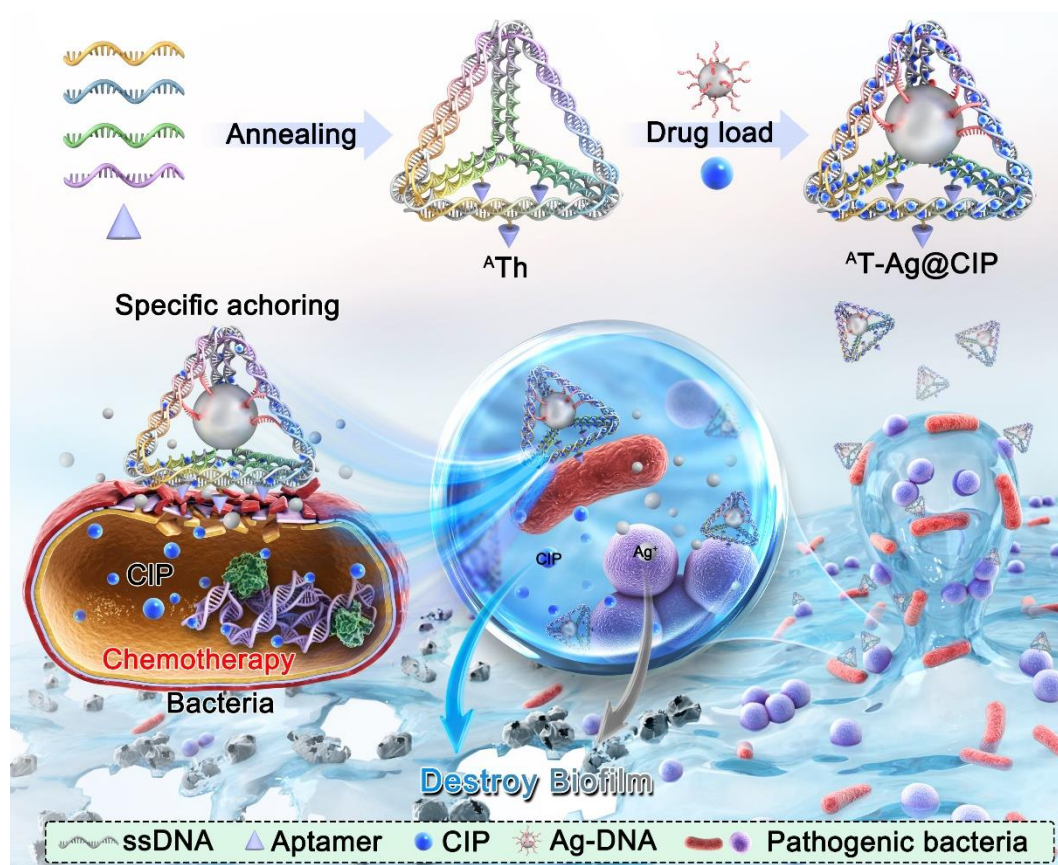54. Y. Liu, Y. Sun, S. Li, M. Liu, X. Qin, X. Chen, Y. Lin, *Nano Lett*. **2020**, *20* 3602.

Figure 1. Schematic illustration of the preparation and anti-bacterial mechanism of the antibiotic-loaded DNA tetrahedron for targeted bacteria killing. [A]Th: double-bundle DNA tetrahedron with bacteria-specific aptamer; [A]T-Ag@CIP: CIP and AgNP co-loaded [A]Th.
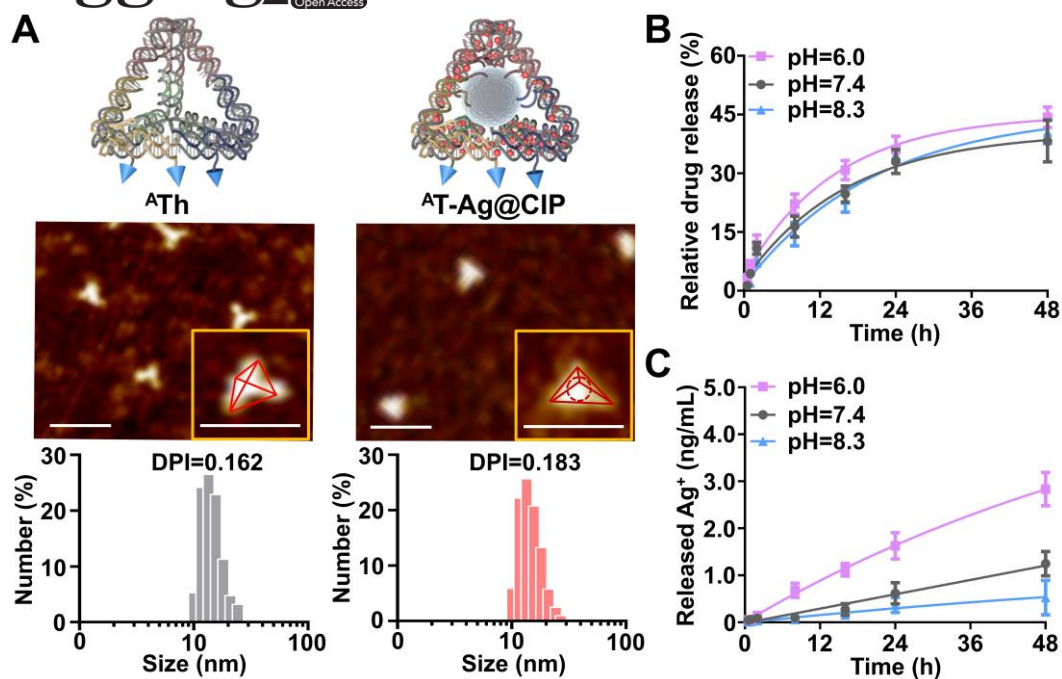
Figure 2. Characterization of the antibiotic-loaded DNA tetrahedron. (A) AFM images and DLS analysis of [A]Th and [A]T-Ag@CIP. (Scale bars: 20 nm). The average diameter of [A]Th and [A]T-Ag@CIP was measured in PBS at room temperature. (B) Sustained CIP release analysis of [A]Th-Ag@CIP in PBS with different pH. (C) Measurement of Ag+ hydrolyzed from [A]T-Ag@CIP in PBS with different pH.
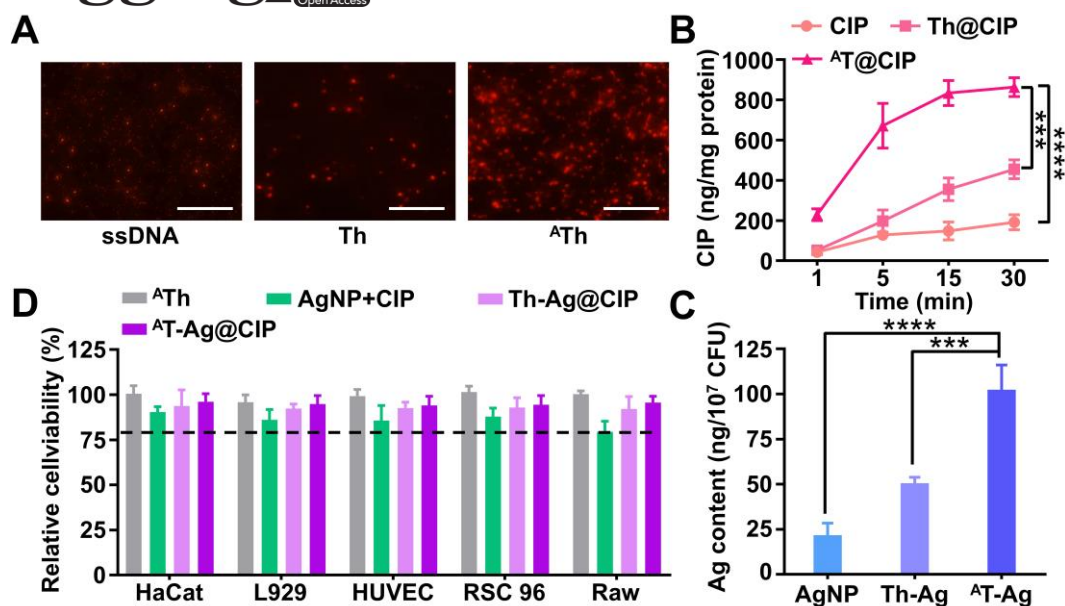
Figure 3. Internalization and biocompatibility of antibiotic-loaded DNA tetrahedron. (A) Confocal images of *E. coil* with indicated treatments for 0.5 h. (Scale bar: 50 μm). (B) Measurement of CIP accumulation in *E. coil* treated with different drugs containing CIP at different times. (C) Accumulation of Ag in *E. coil* after treated with different drugs containing AgNP for 3 h. (D) Cell viability analysis of different cells treated with drugs or drug mixture for 48 h. (***P < 0.001, ****P < 0.0001).
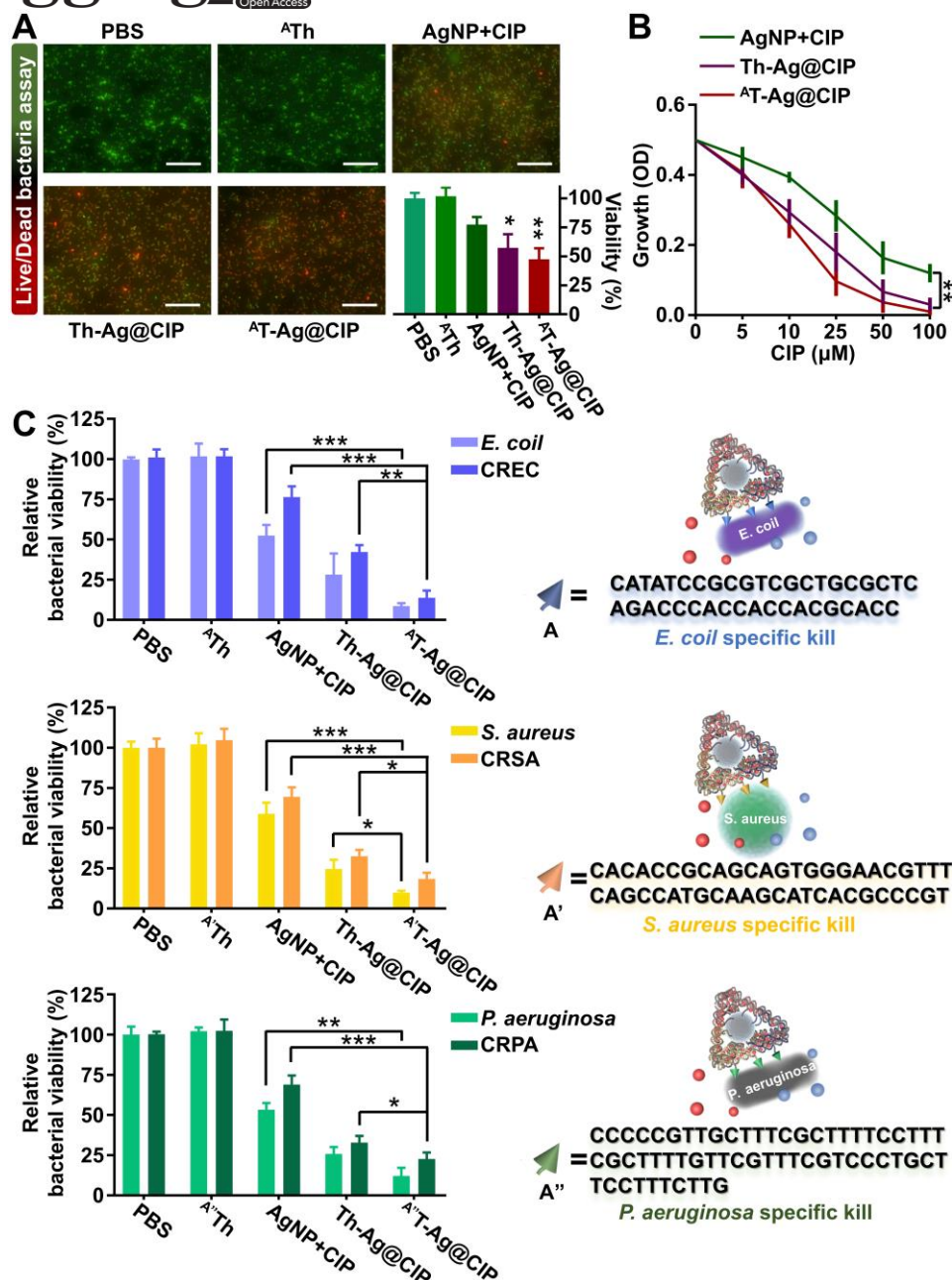
Figure 4. Anti-bacterial effect of the dual-antibiotic delivery system with different targeting aptamer modification. (A) Live/Dead staining of *E. coil* treated with different drugs. Green fluorescence indicates live bacteria; Red fluorescence indicates dead bacteria. (Scale bar: 100 μm). (B) Curves of bacteria growth after treatment with different concentrations of the antibiotic mixture or delivery system. The dosage is based on the concentration of CIP (0-100 μM). (C) Relative bacterial viability analysis of both CIP-sensitive and CIP-resistant bacteria after different treatments. The illustration shows that 3 kinds of bacteria-specific aptamer were

rendered to prepare [A]T-Ag@CIP (for *E. coil* infection), [A']T-Ag@CIP (for *S. aureus* infection), and [A'']T-Ag@CIP (for *P. aeruginosa* infection) separately for different infection therapy. (*P < 0.05, **P < 0.01, ***P < 0.001).
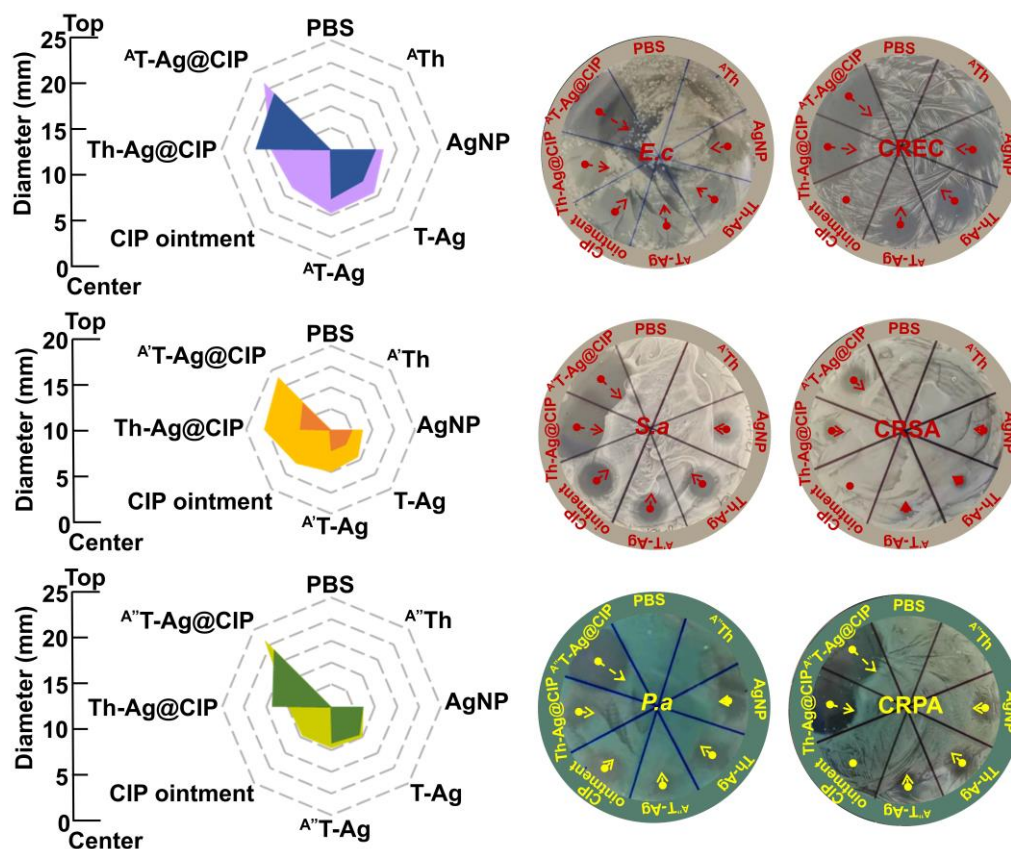

Figure 5. Agar plate diffusion assay of different treatments on CIP-sensitive and CIP-resistant bacteria. The length of the red arrows in the photos indicates the semidiameter of the aseptic area.
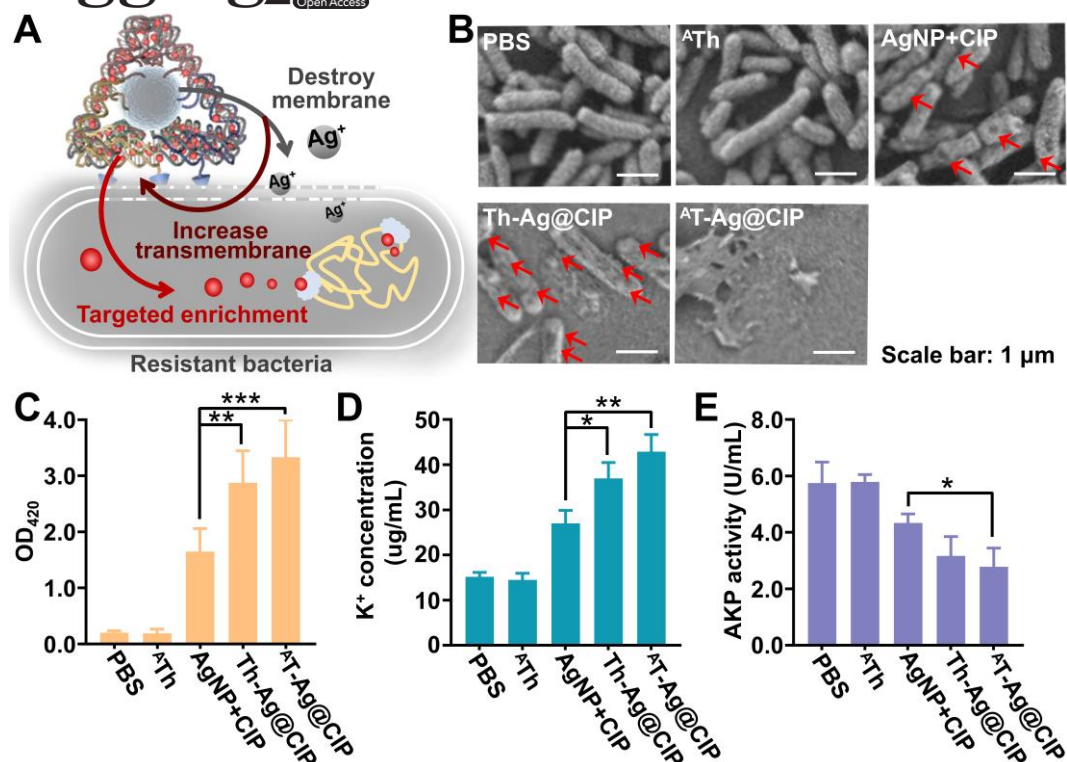
Figure 6. Antibacterial mechanism analysis of [A]T-Ag@CIP. (A) Illustration of the bactericidal mechanism of the dua-antibiotic loaded [A]T-Ag@CIP on bacteria killing. (B) Micromorphologies of CIP-resistant strain CREC treated with different drugs. (Scale bar: 1 μm). (C) ONPG assay of CREC for membrane permeability analysis. (D) Cell leakage analysis of K^{+}. (E) Cell leakage analysis of alkaline phosphatase (AKP). (*P < 0.05, **P < 0.01, ***P < 0.001).
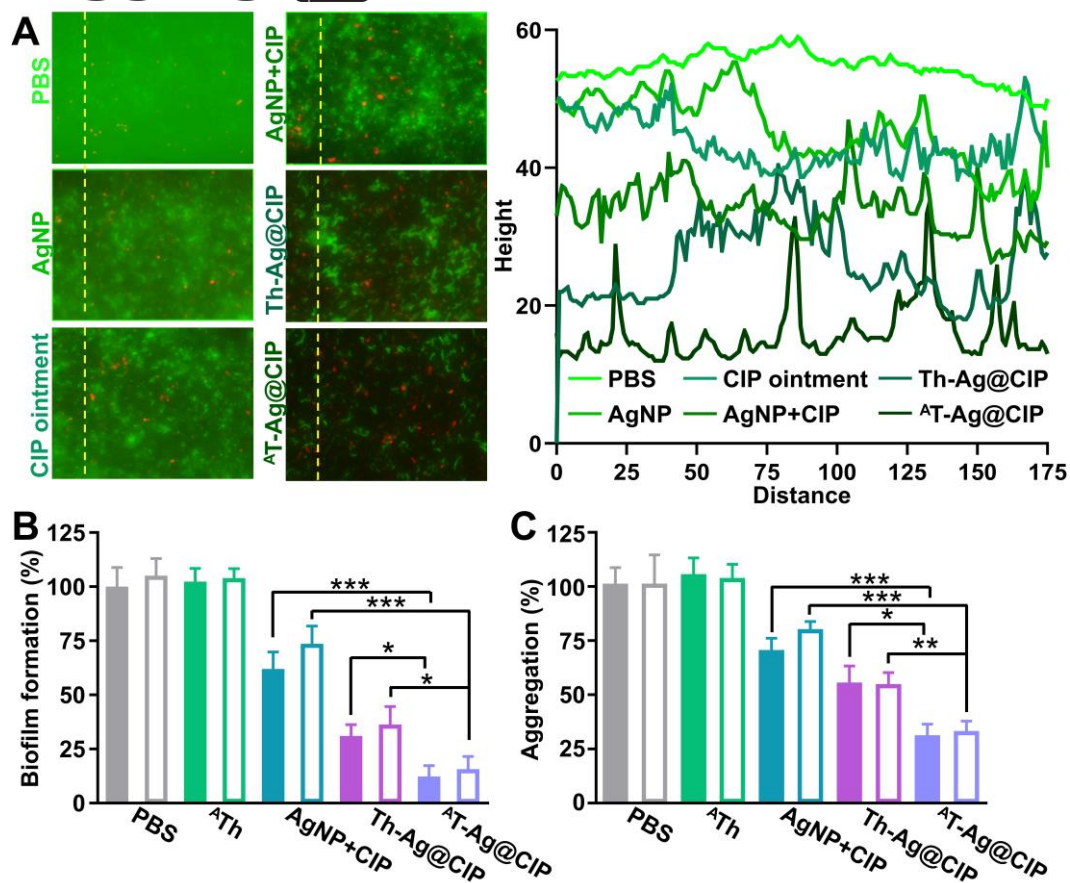
Figure 7. Anti-biofilm analysis of the dual-antibiotic delivery system. (A) Biofilm formation analysis of CREC treated with different drugs. The biofilm was stained by bacterial Live/Dead staining kit. Green fluorescence indicates live bacteria; Red fluorescence indicates dead bacteria. (B) Biofilm inhibition analysis of different drugs and drug mixture. After culture, *E. coil* and CREC biofilm were measured by crystal violet stain. (C) Self-aggregation analysis of *E. coil* and CREC. (*P < 0.05, **P < 0.01, ***P < 0.001).
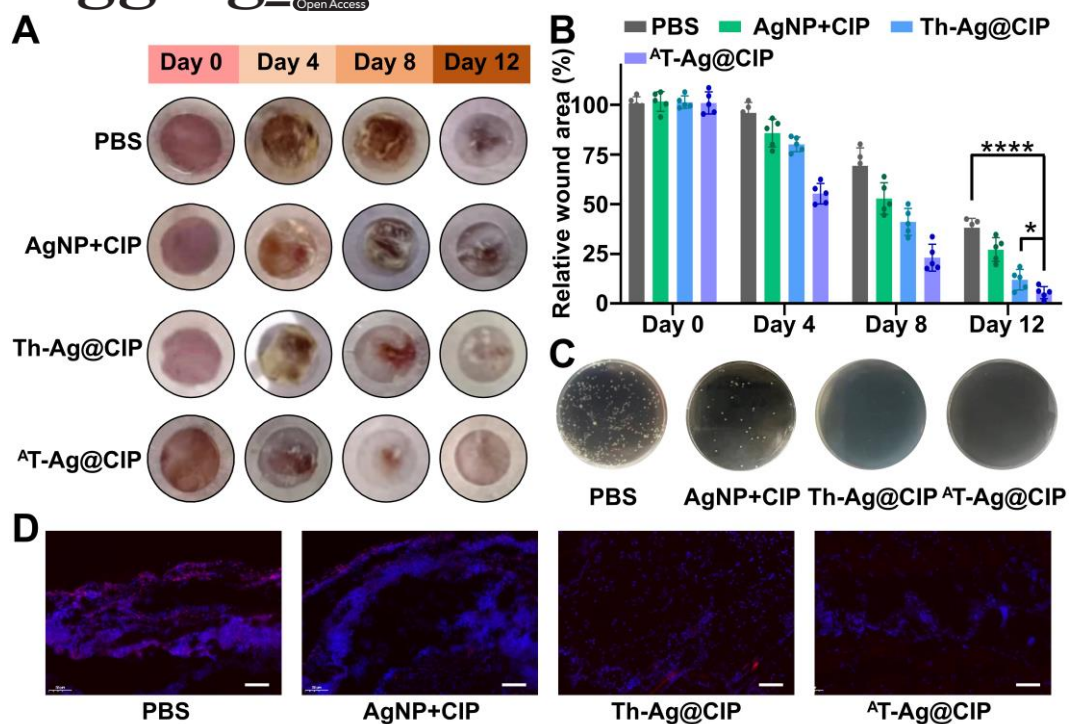
Figure 8. *In vivo* anti-infection therapy. (A) Photographs of the infected wounds of different treatment groups. (B) Quantified wound area on day 0, 4, 8, and 12. (C) Photographs of bacterial colonies from different treatment groups. (D) ROS quantitative imaging of infected skin on Day 4. Red fluorescence signal represents ROS. Blue fluorescence signal represents nucleus stained by DAPI. Scale bar: 30 μm. (*P < 0.05, ***P < 0.001).

A self-assembly DNA tetrahedron-based antibiotic delivery system with precisely organized bacteria-specific aptamer was constructed to achieve targeted delivery of clinical antibiotic ciprofloxacin (CIP) and classic nanoantibiotic silver nanoparticles (AgNP) for the efficient therapy of resistant infection.

Antibiotic resistance, DNA nanotechnology, Targeted delivery, Biofilm, Anti-nfection therapy

Tiantian Wu[1, 2‡], Yu Fu[3‡], Shuang Guo[1‡], Yanqiang Shi[1], Yuxin Zhang[1], Zhijin Fan[1], Bin Yang[1]*, Baoquan Ding[2]* & Yuhui Liao[1]*

Beijing Association on Laboratory Animal Care

Self-assembly multifunctional DNA Tetrahedron for Efficient Elimination of Antibiotic-Resistant Bacteria